




Cite this: *RSC Adv.*, 2020, 10, 6139

# Robust and recyclable sodium carboxymethyl cellulose–ammonium phosphomolybdate composites for cesium removal from wastewater†

Ningluo Zhang, Shangqing Chen, Jiayin Hu, \* Jian Shi, Yafei Guo and Tianlong Deng \*

A novel, facilely prepared, recyclable sodium carboxymethyl cellulose–ammonium phosphomolybdate composite (CMC–AMP) was synthesized by chemical cross-linking and used for Cs<sup>+</sup> removal. The effects of adsorbent dosage, pH value, initial Cs<sup>+</sup> concentration, contact time, temperature and competitive ions on adsorption were investigated. The results showed that CMC–AMP with good mechanical properties could effectively adsorb Cs<sup>+</sup> in a wide pH range. In addition, the adsorption process of CMC–AMP was better fitted with the Lagergren first-second model and Langmuir isotherm model. Furthermore, CMC–AMP can be reused five times using ammonium chloride as the eluent without an obvious decrease in absorption activity. The results reveal that CMC–AMP can be used as a low cost and recyclable Cs<sup>+</sup> adsorbent.

Received 23rd November 2019

Accepted 4th January 2020

DOI: 10.1039/c9ra09803h

rsc.li/rsc-advances

## Introduction

Radioactive cesium (<sup>137</sup>Cs) with a long half-life of 30.1 years and serious gamma radiation is generally caused by nuclear power generation, nuclear wastewater and nuclear accidents, and is an easily diffused pollutant that can accumulate in wildlife and humans, resulting in increasing morbidity of cancer and genetic disorder.<sup>1,2</sup> In particular, after the Fukushima nuclear accident, there was a certain degree of diffusion of <sup>137</sup>Cs into the soil and seawater nearby, resulting in a severe impact on the surrounding environment.<sup>3</sup> Therefore, it is urgent to develop techniques for removing <sup>137</sup>Cs from nuclear wastewater.

At present, there are many developed methods for cesium removal. In view of the characteristics of nuclear wastewater and the concentration of cesium in solution, the adsorption method is more suitable because of its low cost and easy operation.<sup>4</sup> Currently, many adsorbents for cesium removal have been explored, such as Prussian blue (PB),<sup>3,5–7</sup> montmorillonite,<sup>8,9</sup> modified carbon nanotubes,<sup>10,11</sup> zeolites and ammonium phosphomolybdate (AMP).<sup>12–14</sup> Among the previously developed inorganic ion adsorbents, ammonium phosphomolybdate (AMP) is widely used as an ion exchanger because of its excellent selectivity towards cesium ions.<sup>15</sup> More importantly, AMP can be eluted with ammonium salt after adsorbing Cs<sup>+</sup>,<sup>16</sup> which is beneficial for multiple recycling of the adsorbents. However, due

to its microcrystalline structure and fine powder morphology, it is not suitable for direct adsorption.<sup>17</sup> Therefore, many researchers are working on developing supporter materials for immobilizing AMP powders, such as aluminum,<sup>18</sup> polyacrylonitrile,<sup>19</sup> mesoporous silica.<sup>20</sup> Although gratifying progress have been made, there are still some problems in the preparation of these immobilizing materials, such as inferior stability, cumbersome preparation processes and so on. Therefore, the development of robust AMP-based adsorbents with favorable adsorption performance and facile preparation process is still desirable.

Sodium carboxymethyl cellulose (CMC) is a water-soluble cellulose extracted from raw cellulose materials by alkalization or acidification which has been widely used in chemical, light industry, petroleum, food, medicine, and many other fields.<sup>21,22</sup> CMC can form insoluble gel spheres in the presence of multi-valent metal ions such as Fe<sup>3+</sup>, Cu<sup>2+</sup> and Al<sup>3+</sup>.<sup>23–25</sup> Recently, Zong *et al.* synthesized CMC–KCuFC composite microspheres with Cu<sup>2+</sup> as a crosslinking agent, and the particles were able to maintain high stability after separation.<sup>26</sup> However, the secondary pollution caused by the release of trace Prussian blue would lead to serious threat to the water body.<sup>27</sup> In addition, because of the excessive affinity of PB towards Cs<sup>+</sup>, the Cs<sup>+</sup>-laden PB-based adsorbents were difficult to be regenerated and reused, which were not benign in view of economical benefit.

In this study, a robust and recyclable CMC–AMP composite was prepared by immobilizing ammonium phosphomolybdate (AMP) onto sodium carboxymethyl cellulose (CMC) for cesium removal from wastewater. The robust CMC–AMP composite could adsorb Cs<sup>+</sup> at a wide pH range with a maximum adsorption capacity of 65.42 mg g<sup>−1</sup>. More importantly, CMC–AMP can be facilely reused and recycled using ammonium chloride as

Tianjin Key Laboratory of Marine Resources and Chemistry, College of Chemical Engineering and Materials Science, Tianjin University of Science and Technology, Tianjin, 300457, China. E-mail: hujiayin@tust.edu.cn; tldeng@tust.edu.cn

† Electronic supplementary information (ESI) available. See DOI: 10.1039/c9ra09803h



eluent for five times without significant loss in absorption activity and selectivity. Thus, CMC-AMP could be regarded as a potential material for  $^{137}\text{Cs}$  removal from wastewater.

## Experiment

### Materials

All reagents used in the experiments were of analytical grade without further purification. Sodium carboxymethyl cellulose (CMC) was purchased from Tokyo Chemical Industry Co., Ltd. Cesium chloride was obtained from Tianjin Jinke Fine Chemical Research Institute. Ammonium phosphomolybdate (AMP), potassium chloride, sodium hydroxide, ammonium chloride, ferric chloride and hydrochloric acid were supplied by Sino-pharm Reagent Co. Ltd.

For safety reasons, CsCl, a non-radioactive Cs ( $^{133}\text{Cs}$ ), was used in this experiment. 0.1267 g of cesium chloride was dissolved in 1000 mL of deionized water to prepare a  $100\text{ mg L}^{-1}$  Cs $^{+}$  solution. The original solution was diluted into different concentration gradients of cesium chloride solution. The pH values of the solutions were adjusted using  $0.1\text{ mol L}^{-1}$  NaOH and  $0.1\text{ mol L}^{-1}$  HCl and they were measured by a high precision pH meter (PH-7310, WTW Co., Ltd, Germany).

### Preparation of CMC-AMP microspheres

CMC-AMP microspheres were prepared as shown in Fig. 1. First, 1.5 g of AMP powder was weighed and added into 100 mL of deionized water, and 1.5 g of CMC was added to form a uniform yellow sol through mechanical stirring. Then, the mixed sol was gradually dropped into a 2 wt%  $\text{FeCl}_3$  clear solution using a syringe, and yellow microspheres were formed under stirring. The stirring was continued for 12 hours for sufficient crosslinking. Thereafter, the microspheres were washed with deionized water for several times. Finally, the microspheres were dried at  $45\text{ }^{\circ}\text{C}$  for 12 hours for further use.

### Characterization

FT-IR spectra were analyzed at a range of  $4000\text{--}400\text{ cm}^{-1}$ , and the cumulative scan was performed 16 times (Tensor27,

Germany). Surface SEM image analysis was performed on the samples before and after desorption of CMC-AMP microspheres to determine the changes in the morphology of the samples (SEM, JSM-IT300LV, Japan). The elemental composition of the sample was measured by an energy dispersive X-ray spectrometer (EDX, X-Max20, Oxford Instruments).

### Adsorption tests

Batch adsorption tests were conducted in conical flasks containing  $100\text{ mL Cs}^{+}$  solution and a certain mass of adsorbent. All adsorption tests were oscillated on an adjustable temperature water bath shaker at a constant speed of 200 rpm. At a specific time, 2 mL of the solution sample was taken from the flasks and the concentration of Cs $^{+}$  was detected by inductively coupled plasma optical emission spectrometer (ICP-OES, Prodigy, Leeman Corporation, America).

The equilibrium adsorption rate ( $E$ ) and adsorption capacity ( $q_e$ ) of Cs $^{+}$  are calculated using eqn (1) and (2), respectively:

$$E(\%) = \frac{C_0 - C_t}{C_0} \times 100 \quad (1)$$

$$q_e(\text{mg g}^{-1}) = \frac{(C_0 - C_t)V}{m} \quad (2)$$

where  $C_0$  and  $C_t$  are the Cs $^{+}$  concentration at the initial and certain adsorption time  $t$ , respectively;  $V$  (L) is the volume of the solution used for the adsorption tests;  $m$  (g) is the dry weight of the adsorbent.

In order to estimate the affinity and selectivity of the adsorbent for Cs $^{+}$ , the distribution coefficient ( $K_d$ ) was used, and its formula can be expressed as follows:

$$K_d(\text{mL g}^{-1}) = \frac{(C_0 - C_t)}{C_t} \times \frac{V}{m} \quad (3)$$

where  $C_0$  and  $C_t$  are the Cs $^{+}$  concentrations at the initial and equilibrium of the solution after adsorption time  $t$ ;  $V$  (mL) is the volume of the adsorption solution, and  $m$  (g) is the mass of the adsorbent.

### Desorption and reusability

In this study, adsorption-desorption cycles of CMC-AMP was performed to test the reusability of the adsorbent. The adsorption experiment was carried out by using  $100\text{ mL}$  of  $50\text{ mg L}^{-1}$  Cs $^{+}$  solution and a certain amount of adsorbent for 12 h. Then the Cs-containing CMC-AMP was eluted using ammonium chloride. After this, the adsorbent was washed several times with deionized water for the next adsorption-desorption experiment.

## Results and discussion

### Characterization

The FT-IR spectrum of CMC-AMP microspheres is shown in Fig. 2A. It can be found that the broad and strong absorption peaks at  $3430\text{--}3435\text{ cm}^{-1}$  corresponded to the stretching vibration peak of O-H. The weak absorption peak located near  $2921\text{ to }2922\text{ cm}^{-1}$  was the stretching vibration peak of the C-H

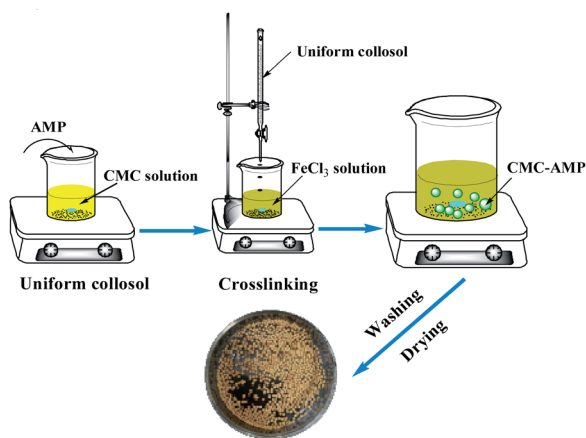


Fig. 1 The preparation process of CMC-AMP spheres.



skeleton (mainly including  $-\text{CH}$  and  $-\text{CH}_2$ ) on the CMC.<sup>28</sup> The four sharp and strong absorption peaks at  $1064.5\text{ cm}^{-1}$ ,  $964.7\text{ cm}^{-1}$ ,  $866.7\text{ cm}^{-1}$ ,  $788.2\text{ cm}^{-1}$  were characteristic peaks of  $[\text{PMo}_{12}\text{O}_{40}]^{3-}$  skeleton of Keggin structure of ammonium phosphomolybdate.<sup>16</sup> This indicated that the AMP was successfully loaded on the CMC substrate. The surface features of the CMC-AMP microspheres were explored using SEM (Fig. 2B). As can be seen from the image, the surface of the CMC-AMP microsphere was wrinkled, which was favorable for adsorption. In addition, energy dispersive X-ray spectroscopy (EDX) was used to analyze the elemental composition of the microspheres. The result is shown in Fig. 2C indicated that the elements of dispersion in CMC-AMP microspheres are C, N, O, P, Mo and Fe, which further verified the successful immobilization of AMP in CMC matrix.

### Effect of CMC-AMP dosage on $\text{Cs}^+$ adsorption

In the adsorption process, it is important to determine the optimum amount of adsorbent. Then, the effect of CMC-AMP dosage on  $\text{Cs}^+$  adsorption were investigated, and the result are shown in Fig. 3. It could be seen that the adsorption efficiency ( $E$ ) increased with the increasing of CMC-AMP dosage. Meanwhile, the adsorption capacity ( $q_e$ ) decreased with the increasing of CMC-AMP dosage, which may be caused by the slower adsorption rate and limited adsorption time. Considering the  $E$  and  $q_e$ , the solid-liquid ratio of the subsequent adsorption experiments was set as  $1\text{ g L}^{-1}$ .

### Effect of solution pH on adsorption

Considering that the pH of the solution has an important effect on adsorption. Therefore, the adsorption experiments with pH value ranging from 2 to 10 were carried out in this experiment, and the results are shown in Fig. 4. CMC-AMP exhibited good stability in the range of pH 2–10. When the pH was lower than 3, the amount of adsorption was obviously low. When pH was larger than 4, the adsorption slightly increased with increasing

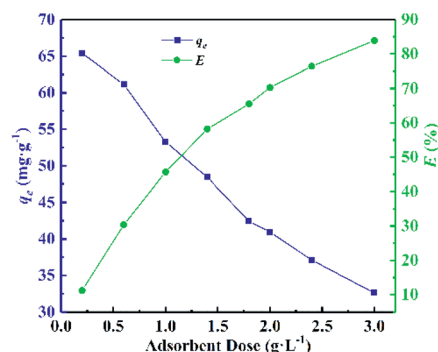


Fig. 3 Effect of adsorbent dosage on  $\text{Cs}^+$  adsorption by CMC-AMP. Adsorption conditions:  $100\text{ mg L}^{-1}\text{ Cs}^+$  concentration, 24 h and  $298.15\text{ K}$ .

pH and then decreased after pH exceeded 8. At low pH, the charge of the CMC-AMP surface was positive, and  $\text{H}^+$  and  $\text{Cs}^+$  were highly competitive for the occupancy of the active sites. Whereas at higher pH values, the charge on the surface of CMC-AMP will become negative, resulting in more active adsorption for  $\text{Cs}^+$ . The decrease in the adsorption capacity after pH 8 attributed to the stronger ion strength.<sup>11</sup>

### Effects of initial concentration of $\text{Cs}^+$ on adsorption and adsorption isotherm

The effects of different initial  $\text{Cs}^+$  concentrations on adsorption capacity at different temperatures were investigated and the results are shown in Fig. 5A. It could be found that the adsorption capacity of  $\text{Cs}^+$  increased with the initial concentration. The reason was that at a lower initial  $\text{Cs}^+$  concentration, the amount of  $\text{Cs}^+$  was insufficient, and many adsorption sites remained unsaturated, so the adsorption capacity was low. When the initial  $\text{Cs}^+$  concentration increased, the adsorption sites became saturated gradually and the adsorption capacity obviously increased. In addition, at different initial  $\text{Cs}^+$  concentrations, the temperature had a positive effect on the adsorption capacity of CMC-AMP, and the maximum adsorption capacity of  $\text{Cs}^+$  at  $323.15\text{ K}$  in 24 h was  $64.20\text{ mg g}^{-1}$ .

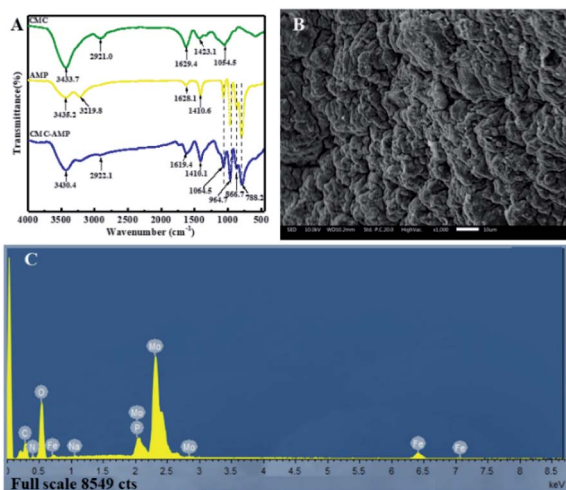


Fig. 2 Characterizations of synthesized CMC-AMP: the FT-IR spectrum (A), representative SEM image (B) and EDX spectrum (C).

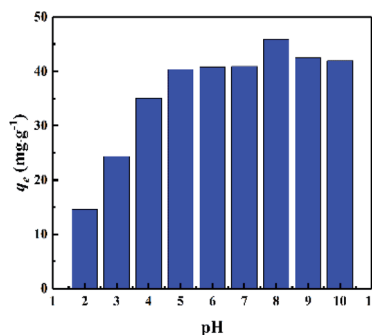


Fig. 4 Effect of pH value on adsorption of  $\text{Cs}^+$ . Adsorption conditions:  $100\text{ mg L}^{-1}\text{ Cs}^+$  concentration, adsorbent dose  $1\text{ g L}^{-1}$ , 24 h and  $298.15\text{ K}$ .



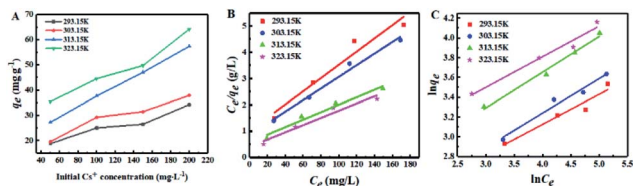


Fig. 5 Effect of initial Cs<sup>+</sup> concentration on adsorption (A) and adsorption isotherm model: Langmuir model (B); Freundlich model (C). Adsorption conditions: adsorbent dose 1 g L<sup>-1</sup>, pH = 7 and 24 h.

In the adsorption process, the equilibrium isotherm is important for providing the information about adsorption mechanism. In this study, the experimental data were processed using the Langmuir and Freundlich models to describe the adsorption of Cs<sup>+</sup> by CMC-AMP in equilibrium state. The linear expressions of the Langmuir and Freundlich models are as follows:<sup>29,30</sup>

Langmuir adsorption isotherm equation

$$\frac{C_e}{q_e} = \frac{1}{bq_{\max}} + \frac{C_e}{q_{\max}} \quad (4)$$

where  $q_e$  (mg g<sup>-1</sup>) is the amount of adsorption for Cs<sup>+</sup> at equilibrium,  $C_e$  (mg L<sup>-1</sup>) is the concentration of Cs<sup>+</sup> in the solution at equilibrium;  $q_{\max}$  is the adsorption capacity for Cs<sup>+</sup> (mg g<sup>-1</sup>),  $b$  is the Langmuir coefficient related to the affinity of the binding site (L mg<sup>-1</sup>).

Freundlich adsorption isotherm equation

$$q_e = K_F C_e^{1/n} \quad (5)$$

$$\ln q_e = \ln K_F + \frac{1}{n} \ln C_e \quad (6)$$

where the eqn (6) is the logarithmic form of the eqn (5).  $K_F$  is the Freundlich adsorption equilibrium constant related to the adsorption capacity;  $n$  is a constant related to the adsorption intensity.

The Langmuir and Freundlich constants are obtained from the slope and intercept calculated in Fig. 5 and the calculated

data is shown in Table S5.† As shown in Table S5,† the adsorption is more likely to follow the Langmuir model ( $R^2 > 0.9522$ ), and the calculated maximum adsorption capacity is 72.89 mg g<sup>-1</sup> at 323.15 K. The above results indicate that the adsorption process is a monolayer adsorption, that is, adsorption mainly occurs on the surface of the adsorbent. For the Freundlich model, the value of  $n$  is 3.286, indicating the favorable adsorption process.

### Effects of contact time on adsorption and adsorption kinetics

The effect of contact time on adsorption of Cs<sup>+</sup> is shown in Fig. 6A. In general, the adsorption capacity of Cs<sup>+</sup> by CMC-AMP increased with increasing adsorption time, and the adsorption capacity reached 61.21 mg g<sup>-1</sup> when the equilibrium state was reached. During the first 60 hours, the adsorption of Cs<sup>+</sup> increased markedly. Then the adsorption rate decreases slightly and finally reached equilibrium. At early stages, there are many available adsorption sites, resulting in a fast adsorption rate. As time increased, the free adsorption sites and the Cs<sup>+</sup> concentration decreased and the adsorption rate became slower.

To further investigate the properties of kinetic adsorption and mechanism, the most widely used kinetic model Lagergren pseudo-first-order and pseudo-second-order was used to evaluate the experimental data.

Lagergren pseudo-first-order kinetic model<sup>31</sup>

$$\ln(q_e - q_t) = \ln q_e - k_1 t \quad (7)$$

where  $q_e$  and  $q_t$  (mg g<sup>-1</sup>) are the amounts of Cs<sup>+</sup> adsorbed at equilibrium and time  $t$ , respectively; and  $k_1$  represents the pseudo-first-order constant. The values of  $k_1$  and  $q_e$  were calculated from the slope and intercept plotted by eqn (7) and shown in Fig. 6B and Table S2.†

Lagergren pseudo-second-order kinetic model<sup>32</sup>

$$\frac{t}{q_t} = \left( \frac{1}{k_2 q_e^2} \right) + \frac{t}{q_e} \quad (8)$$

where  $k_2$  (g mg<sup>-1</sup> min<sup>-1</sup>) represents the pseudo-second-order constant. The values of  $k_2$  and  $q_e$  were calculated from the slope and intercept plotted by eqn (8) and shown in Fig. 6C and Table S3.†

Intra-particle diffusion model<sup>33</sup>

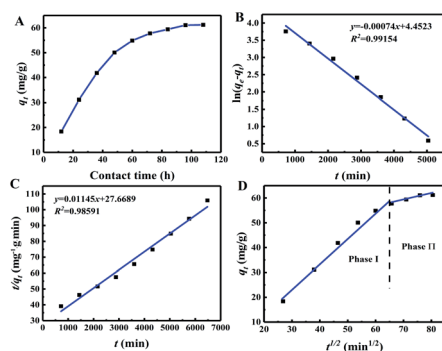


Fig. 6 Effect of contact time on adsorption (A); and kinetic models fitting plots: pseudo-first-order (B); pseudo-second-order (C); intra-particle diffusion (D). Adsorption conditions: 100 mg L<sup>-1</sup> Cs<sup>+</sup> concentration, adsorbent dose 1 g L<sup>-1</sup>, pH = 7 and 298.15 K.

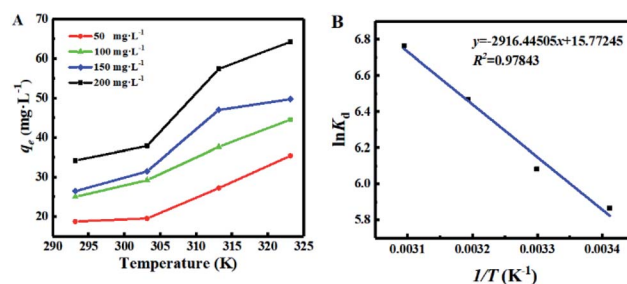


Fig. 7 Effect of temperature on adsorption (A) and thermodynamic fitting (B). Adsorption conditions: adsorbent dose 1 g L<sup>-1</sup>, pH = 7 and 24 h.





$$q_t = k_{\text{dif}} t^{1/2} + C \quad (9)$$

where  $k_{\text{dif}}$  is the intra-particle diffusion rate constant ( $\text{mg g}^{-1} \text{min}^{-1/2}$ ), which can be expressed as the slope of the function.  $C$  is the intercept of the function. The functional relationship between  $q_t$  and  $t^{1/2}$  is shown in Fig. 6D, and the relevant model parameters are listed in Table S4.†

The calculation shows that the correlation coefficient of the pseudo first-order model is higher than that of the pseudo second-order model. Furthermore, it was found that the  $q_t$  of CMC-AMP is multi-linear for the intra-particle diffusion model of  $t^{1/2}$  and can be divided into two phases (Fig. 6D). Stage I refers to diffusion from the bulk solution to the surface of the adsorbent. Stage II represents the diffusion of ions within the microporous crystals of CMC-AMP. For the intra-particle rate constant,  $k_{\text{dif1}}$  is much higher than  $k_{\text{dif2}}$ , and surface diffusion is an instantaneous diffusion phase.<sup>34</sup> Due to the larger correlation coefficient, the adsorption process is more in line with pseudo first-order model, indicating that the main adsorption mechanism of  $\text{Cs}^+$  on CMC-AMP is chemisorption.

### Effects of temperature on adsorption and adsorption thermodynamics

During the adsorption process, temperature has an important effect on the adsorption effect by affects the diffusion rate of ions in the solution. Thus, the adsorption of  $\text{Cs}^+$  at a solution temperature of 293.15 K to 323.15 K were carried out. As shown in Fig. 7A, at the different initial concentration, when the temperature increased from 293.15 K to 323.15 K, the adsorption of  $\text{Cs}^+$  by CMC-AMP microspheres increased with the increasing temperature, indicating that the adsorption process was an endothermic reaction. However, in order to reduce energy consumption, the other experiments were carried out at room temperature.

In order to further explore the thermodynamic properties of the adsorption process, enthalpy ( $\Delta H^0$ ,  $\text{kJ mol}^{-1}$ ), entropy ( $\Delta S^0$ ,  $\text{J mol}^{-1} \text{K}^{-1}$ ), and Gibbs free energy ( $\Delta G^0$ ,  $\text{kJ mol}^{-1}$ ) were studied in this experiment. And they are calculated by the following equations:<sup>16</sup>

$$\ln K_d = \frac{\Delta S^0}{R} - \frac{\Delta H^0}{R} \times \frac{1}{T} \quad (10)$$

$$\Delta G^0 = \Delta H^0 - T\Delta S^0 \quad (11)$$

where  $K_d$  is the equilibrium distribution coefficient,  $T$  (K) is the thermodynamic temperature, and  $R$  is the general gas constant, which is  $8.314 \text{ J mol}^{-1} \text{K}^{-1}$ , respectively.

The values of  $\ln K_d$  were obtained at different temperatures. According to the results shown in Fig. 7B, the values of  $\Delta H^0$  and  $\Delta S^0$  are calculated as  $24.25 \text{ kJ mol}^{-1}$  and  $131.13 \text{ J mol}^{-1} \text{K}^{-1}$ , respectively. The values of  $\Delta G^0$  at different temperatures were calculated by eqn (11), and the thermodynamic parameters were shown in Table S1 (see ESI).†

The value of  $\Delta H^0$  was positive in the adsorption of  $\text{Cs}^+$  by CMC-AMP, indicating that the adsorption was an endothermic process, which was consistent with the experimental results of Fig. 7. In addition, all  $\Delta G^0$  values were negative at temperatures from 293.15 to 323.15 K, so the adsorption process of  $\text{Cs}^+$  by CMC-AMP was thermodynamically feasible and spontaneous in nature.

### Effects of competing ions on adsorption

In nuclear wastewater, the presence of alkali and alkaline earth metal ions (*e.g.*  $\text{Li}^+$ ,  $\text{Na}^+$ ,  $\text{K}^+$ ,  $\text{Mg}^{2+}$  and  $\text{Ca}^{2+}$ ) affects the absorption of  $\text{Cs}^+$ . Among them,  $\text{K}^+$  has the greatest effect on the adsorption of  $\text{Cs}^+$  since there is a close radius between  $\text{K}^+$  and  $\text{Cs}^+$ .<sup>35</sup> Therefore, in this experiment,  $\text{K}^+$  was selected as the competitive ion of  $\text{Cs}^+$  to explore the adsorption selectivity of CMC-AMP. In the test of selective adsorption, the concentrations of  $\text{K}^+$  were ranged from 20 to 200  $\text{mg L}^{-1}$  and the concentration of  $\text{Cs}^+$  was kept at  $100 \text{ mg L}^{-1}$ . The result in Fig. 8 showed that as the concentration of  $\text{K}^+$  increased, the adsorption efficiency and distribution coefficient  $K_d$  of  $\text{Cs}^+$  decreased. However, the distribution coefficients of  $\text{Cs}^+$  were always above  $4 \times 10^2$ , indicating the good selectivity of CMC-AMP for  $\text{Cs}^+$ . Moreover, the adsorption in ground water (Table S7†) further suggest the potential application of CMC-AMP in  $\text{Cs}^+$  adsorption in real water.

### Desorption and reusability

After adsorption, the cesium-laden CMC-AMP (CMC-AMP-Cs) was eluted using  $\text{NH}_4\text{Cl}$  as a desorption solution. Firstly, the

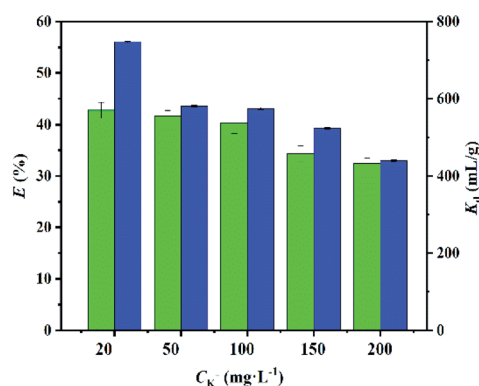


Fig. 8 Effect of competing ions on  $\text{Cs}^+$  adsorption by CMC-AMP. Adsorption conditions:  $\text{Cs}^+$  concentration  $100 \text{ mg L}^{-1}$ , adsorbent dose  $1 \text{ g L}^{-1}$ ,  $\text{pH} = 7$ , 24 h and  $298.15 \text{ K}$ .

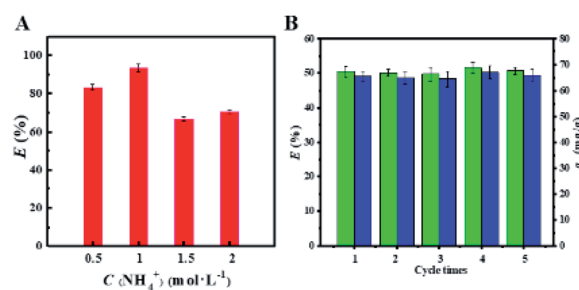


Fig. 9 Effect of different concentrations of  $\text{NH}_4\text{Cl}$  on the elution of cesium from CMC-AMP (A); regeneration performance of CMC-AMP for five consecutive times (B).



**Table 1** Comparison between synthesis mechanism, synthesis process and adsorption capacity of Cs<sup>+</sup> uptake on various AMP composite materials

Materials	Synthesis mechanism	Synthesis conditions	Adsorption capacity (mg g <sup>-1</sup> )	Ref.
Pure AMP	—	—	87.7–135.6	36
AMP/alumina	Gel entrapment	Heated to 95 °C	10–12	18
AMP/zirconium phosphate	Precipitation	Digested at 50 °C under stirring	7.7	37
AMP/silica	Cross-linked	Heated to 90 °C and sol-gel for 3 days	37.63 ± 0.38	38
SM-AMP20	Sequential annealing	Heated to 90 °C and sequential cooling	15.48	39
AMP/silica gel	Coagulation	Heated to 90 °C and washed with trichloroethylene	47.84	40
CMC-AMP	Cross-linked	Room temperature	65.4	This work

effect of NH<sub>4</sub>Cl concentrations on the desorption performance was studied. It can be seen from Fig. 9A that as the concentration of NH<sub>4</sub>Cl solution increased, the desorption rate of Cs<sup>+</sup> firstly increased and then decreased. When the concentration of NH<sub>4</sub>Cl solution was 1 mol L<sup>-1</sup>, the desorption rate of Cs<sup>+</sup> was the highest, which was 93.27%. Therefore, 1 mol L<sup>-1</sup> NH<sub>4</sub>Cl solution was selected as the eluent.

After desorption, the adsorbent was washed for several times with deionized water for the next use. A total of 5 adsorption-desorption cycles were performed to test the reusability and stability of the adsorbent. Fig. 9B shows that there was almost no decrease in adsorption capacity over multiple cycles, and CMC-AMP remained stable during this process. This indicates that CMC-AMP composites have good reusability in cycle experiments, which helps to reduce the cost in application.

The CMC-AMP after five-times reused were characterized by FT-IR, SEM and EDX to further determine their stability. The FT-IR spectra in Fig. S1A† showed that there was no significant change in the CMC-AMP stretching vibration peak before (a) and after (b) desorption, indicating that the chemical structure of the adsorbent did not change obviously after the desorption experiment. The SEM image (Fig. S1B†) shows that the surface of CMC-AMP was slightly rougher than that before absorption. EDX analysis showed that the signal of element cesium was clearly observed on the surface of CMC-AMP-Cs (Fig. S1C and Table S6†), which further suggest the affinity of CMC-AMP toward Cs<sup>+</sup>.

### Comparison of various adsorbents for Cs<sup>+</sup>

The adsorbents synthesized in this work were compared with the reported materials to evaluate the performance of CMC-AMP and the results are shown in Table 1. It was found that the CMC-AMP developed in this study had lower reaction temperature and mild reaction conditions than other reported AMP composites, indicating that the method was cost effective and easy to be popularized. In addition, the adsorption capacity of CMC-AMP was comparable and much larger than some AMP-based composites. In summary, CMC-AMP could be accepted as a promising adsorbent with potential application in cesium removal from wastewater.

## Conclusions

In this study, a robust and recyclable CMC-AMP composite adsorbent was prepared for Cs<sup>+</sup> removal from aqueous solution.

Under the optimal adsorption conditions, the maximum adsorption capacity of the CMC-AMP could reach 64.20 mg g<sup>-1</sup>. The composite could effectively adsorb Cs<sup>+</sup> at a wide range of pH value and the adsorption process was found to be spontaneous and endothermic. The investigated adsorption processes fit pseudo first-order model and Langmuir isotherms respectively. In the presence of K<sup>+</sup>, the distribution coefficients of Cs<sup>+</sup> were always relatively high, indicating that CMC-AMP was highly selective for Cs<sup>+</sup>. More importantly, CMC-AMP had high reusability and stability and could be efficiently eluted and recovered by ammonium chloride solution, and reused for five times without significant loss in adsorption properties. Therefore, the CMC-AMP composite are expected to be with potential applications in the treatment of Cs<sup>+</sup> from nuclear wastewater.

## Conflicts of interest

There are no conflicts to declare.

## Acknowledgements

The authors gratefully acknowledge partial financial support from the National Natural Science Foundation of China (U1607123 and 21773170), the Open Foundation of Tianjin Key Laboratory of Marine Resources and Chemistry (201701), the Yangtze Scholars and Innovative Research Team of the Chinese University (IRT\_17R81) and the Key Projects of Natural Science Foundation of Tianjin (18JCZDJC10040).

## Notes and references

- 1 S. M. Park, J. Lee, E. K. Jeon, S. Kang, M. S. Alam, D. C. W. Tsang, D. S. Alessi and K. Baek, *Geoderma*, 2019, **340**, 49–54.
- 2 J. C. Leaphart, K. C. Wilms, A. L. Bryan and J. C. Beasley, *J. Environ. Radioact.*, 2019, **203**, 25–29.
- 3 M. Kotomi, A. A. Mariko, M. Takeshi and K. Jun, *J. Environ. Radioact.*, 2019, **208–209**, 106040.
- 4 J. F. Zhang, L. R. Yang, T. T. Dong, F. Pan, H. F. Xing and H. Z. Liu, *Ind. Eng. Chem. Res.*, 2018, **57**, 4399–4406.
- 5 A. Nilchi, B. Malek, M. G. Maragheh and A. Khanchi, *J. Radioanal. Nucl. Chem.*, 2003, **258**, 457–462.
- 6 Y. C. Lai, Y. R. Chang, M. L. Chen, Y. K. Lo, J. Y. Lai and D. J. Lee, *Bioresour. Technol.*, 2016, **214**, 192–198.



- 7 G. R. Chen, Y. R. Chang, X. Liu, T. Kawamoto, H. Tanaka, D. Parajuli, M. L. Chen, Y. K. Lo, Z. F. Lei and D. J. Lee, *Sep. Purif. Technol.*, 2015, **153**, 37–42.
- 8 B. Ma, S. Oh, W. S. Shin and S. J. Choi, *Desalination*, 2011, **276**, 336–346.
- 9 H. A. Alamudy and K. Cho, *Chem. Eng. J.*, 2018, **349**, 595–602.
- 10 R. Yavari, Y. D. Huang and S. J. Ahmadi, *J. Radioanal. Nucl. Chem.*, 2011, **287**, 393–401.
- 11 I. M. Abdelmonem, E. Metwally, T. E. Siyam, F. A. El-Nour and A. R. M. Mousa, *J. Radioanal. Nucl. Chem.*, 2019, **319**, 1145–1157.
- 12 W. Baek, S. Ha, S. Hong, S. Kim and Y. K. Kim, *Microporous Mesoporous Mater.*, 2018, **264**, 159–166.
- 13 S. Q. Chen, J. Y. Hu, J. Shi, M. X. Wang, Y. F. Guo, M. L. Li, J. Duo and T. L. Deng, *J. Hazard. Mater.*, 2019, **371**, 694–704.
- 14 X. S. Ye, Z. J. Wu, W. Li, H. N. Liu, Q. Li, B. J. Qing, M. Guo and F. Ge, *Colloids Surf., A*, 2009, **342**, 76–83.
- 15 J. Van and R. Smit, *Nature*, 1958, **181**, 1530–1531.
- 16 H. J. Yang, H. W. Yu, J. K. Sun, J. T. Liu, J. B. Xia, J. D. Fang, Y. Li, F. Z. Qu, A. Y. Song and T. Wu, *Chem. Eng. J.*, 2017, **317**, 533–543.
- 17 J. Krttil, *J. Inorg. Nucl. Chem.*, 1962, **24**, 1139–1144.
- 18 R. Chakravarty, R. Ram, K. T. Pillai, Y. Pamale, R. V. Kamat and A. Dash, *J. Chromatogr. A*, 2012, **1220**, 82–91.
- 19 Y. Park, Y. C. Lee, W. S. Shin and S. J. Choi, *Chem. Eng. J.*, 2010, **162**, 685–695.
- 20 Y. Park, W. S. Shin and S. J. Choi, *Chem. Eng. J.*, 2013, **220**, 204–213.
- 21 M. Hashem, S. Sharaf, M. M. A. El-Hady and A. Hebeish, *Carbohydr. Polym.*, 2013, **95**, 421–427.
- 22 X. J. Wang, Li Liu, S. Q. Xia, B. Muhoza, J. B. Cai, X. M. Zhang, E. Duhoranimana and J. k. Su, *Food Hydrocolloids*, 2019, **93**, 10–18.
- 23 J. Y. Hu, S. Q. Chen, N. L. Zhang, Z. Wang, J. Shi, Y. F. Guo and T. L. Deng, *New J. Chem.*, 2019, **43**, 9658.
- 24 Y. L. Zong, Y. D. Zhang, X. Y. Lin, D. Ye, D. Qiao and S. N. Zeng, *RSC Adv.*, 2017, **7**, 31352–31364.
- 25 S. Barkhordari and M. Yadollahi, *Appl. Clay Sci.*, 2016, **121–122**, 77–85.
- 26 Y. L. Zong, Y. D. Zhang, X. Y. Lin, *et al.*, *RSC Adv.*, 2017, **7**, 31352–31364.
- 27 Y. C. Lai, Y. R. Chang, M. L. Chen, *et al.*, *Bioresour. Technol.*, 2016, **214**, 192–198.
- 28 M. Anna, C. Ewa, K. Anna and Z. Marian, *Food Chem.*, 2014, **156**, 353–361.
- 29 I. Langmuir, *J. Am. Chem. Soc.*, 1918, **40**, 1361–1403.
- 30 O. Nakahara, *Soil Sci. Plant Nutr.*, 1996, **42**, 41–49.
- 31 Y. H. Liu, L. Guo, L. L. Zhu, X. Q. Sun and J. Chen, *Chem. Eng. J.*, 2009, **158**, 108–114.
- 32 P. A. Kumar, M. Ray and S. Chakraborty, *Chem. Eng. J.*, 2008, **149**, 340–347.
- 33 Q. Li, J. Zhai, W. Zhang, *et al.*, *J. Hazard. Mater.*, 2007, **141**, 163–167.
- 34 S. M. Robinson, W. D. Arnold and C. H. Byers, *AIChE J.*, 2010, **40**, 2045–2054.
- 35 X. F. Yi, F. L. Sun, Z. H. Han, F. H. Han, J. R. He, M. R. Ou, J. J. Gu and X. P. Xu, *Ecotoxicol. Environ. Saf.*, 2018, **158**, 209–318.
- 36 D. Alby, C. Charnay, M. Héran, *et al.*, *J. Hazard. Mater.*, 2017, **344**, 511.
- 37 G. Murthy, M. Sivaiah, S. Kumar, *et al.*, *J. Radioanal. Nucl. Chem.*, 2004, **260**, 109–114.
- 38 H. Deng, Y. Li, Y. Huang, *et al.*, *Chem. Eng. J.*, 2016, **286**, 25–35.
- 39 H. Deng, Y. Li and L. Wu, *J. Hazard. Mater.*, 2016, **324**, 348.
- 40 J. Doležal, J. Stejskal, M. Tympl and V. Kouřim, *J. Radioanal. Chem.*, 1974, **21**, 381–387.

